Nonsense-mediated decay controls a negative feedback loop in innate immune sensing

Simon Boudreault[1], Yahira Rivera-Lopez[1], Max B Ferretti[1], James Bonner[2], Bertram L Jacobs[2], Kristen W Lynch[1,*]

[1] Department of Biochemistry and Biophysics, University of Pennsylvania, Philadelphia, USA, 19104.

[2] ASU-Banner Center for Neurodegenerative Diseases and School of Life Sciences, Arizona State University, Tempe, USA, 85287.

*Correspondence:

Kristen W Lynch
Department of Biochemistry and Biophysics
Stellar-Chance Labs 909B
422 Curie Blvd
Philadelphia, PA 19104-6059
Office: 215-573-7749
Fax: 215-573-8899
Email: klync@pennmedicine.upenn.edu
klync@pennmedicine.upenn.edu

ABSTRACT

Nonsense-mediated decay (NMD) is an mRNA decay pathway which degrades potential harmful transcripts that contain premature termination codons. However, NMD's importance also extends to the control of isoform abundance under physiological conditions. During viral infection, NMD is inhibited through numerous mechanisms; however, NMD has been shown to have both antiviral as well as proviral activities, raising further questions into the role and control of NMD during viral infection. These observations have led us to investigate the potential involvement of NMD in dsRNA sensing as a mechanism that might explain these discrepancies. Using EIF4A2 exon 10B inclusion as an example of AS-NMD isoform accumulating during viral infection, we show that dsRNA sensing inhibits NMD. This effect is correlated with translational blockade and is driven primarily by RNaseL activation, and by PKR in the absence of RNaseL activation. Surprisingly, NMD promotes the induction of IFN-β as well as interferon-stimulated genes, and this effect is upstream of IRF3 translocation to the nucleus. NMD also promotes RNaseL activation, suggesting NMD directly controls dsRNA sensing. Therefore, inhibition of NMD upon dsRNA sensing provides a negative feedback loop that contributes to shaping the innate immune sensing pathways.

INTRODUCTION

Nonsense-mediated decay (NMD) is an eukaryotic translation-dependant mRNA decay pathway that detects and targets transcripts with unusual features for degradation[1]. Activation of NMD requires the recruitment and phosphorylation of the UPF1 helicase by the SMG1 kinase, usually downstream of a translation termination codon, as the first step to commit the transcript to decay[2,3]. Decay can then occurs through two different pathways, either by endonucleolytic cleavage mediated by SMG6, or recruitment of the CCR4/NOT complex for deadenylation through SMG5 and SMG7[4]. A major feature that induces NMD is the presence of an exon-junction complex downstream of the termination codon, which indicates the presence of a premature stop codon. In addition, the length of the 3'-UTR, RNA structures, and binding of RNA-binding proteins all contributes to the sensitivity to NMD. The complex interplay between all these factors ultimately dictates whether the transcript is targeted by NMD, and the extent to which decay occurs[5].

It has been estimated that NMD controls the expression of roughly 10% of endogenous unmutated mammalian mRNA to fine-tune their levels to various physiological conditions[6]. One way in which unmutated transcripts are targeted by NMD is via alternative splicing in a process called AS-NMD, in which introduction or removal of coding regions by alternative splicing will lead to a premature termination codon that is then sensed by the NMD machinery[7–9]. Thus, products of alternative splicing that do not encode a full-length protein are removed from the transcriptome. Although viruses have been shown to trigger widespread alternative splicing changes during infection, the extent to which these splicing events are targets of NMD has not been thoroughly explored[10–14].

Despite a dearth in investigation of AS-NMD during viral infection, the importance of NMD during viral infection has been clearly established in recent years. NMD usually exerts an antiviral effect on viruses, especially RNA viruses with a positive sense single-stranded genome (+ssRNA viruses), including

flaviviruses and Semliki Forest virus[15–20]. Viral RNA from these viruses exhibits NMD-triggering features and are often subject to NMD degradation. Consequentially, numerous viruses have been shown to directly target the NMD machinery to inhibit this antiviral process. For example, the capsid protein of Semliki Forest virus interacts with NMD components and can inhibit NMD upon ectopic expression[21]; UPF1 is targeted by the nucleocapsid of SARS-CoV-2[22,23]; and the exon-junction complex protein PYM1 is targeted by flaviviruses capsid proteins to inhibit NMD[16]. However, PYM1 is also a proviral factor during another flavivirus infection, Hepatitis C virus (HCV), raising questions about the broader role of NMD during viral infection[24]. UPF1 is also proviral for human immunodeficiency virus (HIV)[25], and negative-strand RNA viruses (−ssRNA viruses) such as Influenza A virus (IAV) and respiratory syncytial virus are not sensitive to the effects of NMD[26]. These conflicting results about the function of NMD during viral infections suggest a more intricate and wider role of NMD during virus-host interactions that requires further studies.

Virus-host interactions describe the complex relationship between the host cell and the invading pathogen, which will ultimately dictate the outcome of infection. During their replication cycle, viruses produce a plethora of pathogen-associated molecular patterns (PAMP), such as incompletely capped mRNA and dsRNA, that are sensed by various host receptors to mount an efficient antiviral response. Upon sensing of dsRNA, the response can be divide into three main arms: (1) activation of the interferon (IFN) response pathway through RIG-I and MDA-5, leading to the production and secretion of IFN-β that stimulate the induction of interferon-stimulated genes (ISG) that are mostly antiviral[27]; (2) activation of the OAS-RNaseL system, in which RNaseL cleaves mRNA, rRNA, as well as viral RNA to inhibits translation and impair viral replication[28]; and (3) activation of PKR, which phosphorylates EIF2α to impair translation[29]. The contribution of NMD to these antiviral responses has not been deciphered.

In the present study, we demonstrate a broad program of AS-NMD in response to both viral infection and dsRNA sensing. We then investigate the drivers and impact of NMD upon dsRNA sensing, using EIF4A2 exon 10B inclusion as an example of AS-NMD. We show that dsRNA sensing inhibits NMD, mainly through RNaseL activation, and NMD inhibition itself restricts the IFN response as well as RNaseL activation triggered by dsRNA. These data reveal a negative feedback loop involving NMD in dsRNA sensing that contributes to shaping the innate immune sensing pathways.

MATERIAL AND METHODS

Cells, drugs, and viruses

A549 were grown in RPMI medium (Corning, 10-040-CV) supplemented with 10% heat-inactivated fetal bovine serum (FBS) (Gibco, A56697-01), and 2 mM penicillin-streptomycin (Mediatech, MT-30-002-Cl). The generation of OAS1, OAS2, OAS3, RNaseL, and PKR KO A549 cells was described before[30,31]. HEK 293T were grown in DMEM (Corning, 10-013-CV) supplemented with 10% FBS, 2 mM penicillin-streptomycin. L929 were grown in EMEM (ATCC, 30-2023) supplemented with 5% FBS and 2 mM penicillin-streptomycin. All cell lines were maintained at 37°C in a humidified incubator with 5% CO_2. Cycloheximide (CHX, MilliporeSigma) and homoharringtonine (HHT, Abcam) were diluted in DMSO and used at a final concentration of 100 µg/mL (CHX) or 2 µg/mL (HHT). hSMG-1 inhibitor 11j (SMG1i, MedChemExpress) was diluted in DMSO and used at 3 µM, except where indicated. Okadaic Acid and Calyculin (Millipore Sigma) were diluted in DMSO and used at 500 nM and 50 nM, respectively. Vesicular stomatitis virus harboring eGFP (VSV-GFP) was kindly provided by Dr. John K. Rose. Mayaro virus (MAYV, strain BeH407), Zika virus (ZIKV, strain MR766), and Rift Valley Fever virus (RVFV, strain MP12) were gifts from Dr. Michael Diamond. West Nile virus (WNV, KUNV isolate CH16532) was a generous gift of Dr. Robert Tesh. Chikungunya virus (CHIKV, strain Ross) was provided by Dr. David Weiner (University of Pennsylvania). Influenza A virus (IAV) used in this manuscript is A/WSN/33 (WSN). CHIKV, MAYV, WNV, and ZIKV were all propagated in C6/36 mosquito cells. RVFV and VSV-GFP were propagated in BHK-21 cells. IAV was propagated in MDCK cells. Supernatants were collected, aliquoted and subjected to only a single freeze-thaw. Viral titers were determined by plaque assays on BHK-21, Vero-E6 cells, or MDCK cells. Vaccinia virus (VACV, Copenhagen strain, VC-2) and the ΔE3L mutant[32] were propagated and titered as previously described[33]. VSV-GFP was UV-inactivated in 1.5 mL tubes, lid opened, 100 µL/tube, under a 254 nm handheld UV lamp (UVP UVG-11, Analytikjena) for 15 min. Controls were infected for longer timepoints alongside the experiment and monitored for GFP expression to validate abrogation of viral

replication. Human IFN-β recombinant protein (ThermoFisher, 300-02BC) was used at 100 units/mL for 5h.

Transfection of PAMP and siRNA

PAMP were bought from Invivogen: Poly(I:C) HMW (tlrl-pic); Poly(I:C) LMW (tlrl-picw), Poly(A:U) (tlrl-pau), 5'-OH-dsRNA (tlrl-3prnac), 5'-PPP-dsRNA (tlrl-3prna), 5'-PPP-hpRNA (tlrl-hprna) and Poly(dA:dT) (tlrl-patn). Poly(I:C) HMW was used except where indicated. For PAMP transfection, 1 µg of the PAMP was transfected using 3 µL of Lipofectamine2000 (ThermoFisher Scientific) in a 12-well plate or scaled accordingly and RNA harvested after 6h. For siRNA transfection, 10 pmoles of siRNA was transfected using 3 µL of RNAiMAX (ThermoFisher Scientific) in 12-well plate or scaled accordingly. Cells were incubated for 72 h to allow complete depletion of the siRNA target. ON-TARGETplus SMARTpool siRNA were purchased from Horizon Discovery against PKR (L-003527), RNaseL (L-005032), or non-targeting control (D-001810-10).

RNA extraction

Total RNA was extracted using TRIzol (Invitrogen) according to the manufacturer's instructions.

Radioactive RT-PCR

Low-cycle radioactive RT-PCR were conducted as previously described[34,35]. 250 ng of RNA was reverse transcribed using MMLV reverse transcriptase (ThermoFisher) using the same reverse primer used for the PCR step. Primer sequences are listed in Supplementary Table 1. PCR reactions were carried out for between 20 to 25 cycles depending on the target. Amplicons were resolved on a 5% denaturing polyacrylamide-Urea gel, densitometry measured using a Typhoon PhosphorImager (Amersham Biosciences) and quantitated using Fiji.

qPCR

The complete list of primers used in this study is available in Supplementary Table 1. Reverse transcription was done using 1 µg of RNA, random hexamers (Invitrogen), and the MMLV reverse transcriptase (Thermo, 28025013). cDNA was diluted to 5 ng/µL following the RT step. Quantitative PCR (qPCR) reactions were prepared in 10 µl in 384-well plates with 5 µL of SYBR qPCR Master Mix (Applied Biosystems, A25742), 2 µL of cDNA (10 ng), 0.4 µL of the primer pair at 10 µM, and 2.6 µL of water. qPCR reactions were carried on a QuantStudio 6 Flex Real-Time PCR System (Applied Biosystems) and data acquired with QuantStudio 12K Flex software version 1.3 (Applied Biosystems). ACTB was used for normalization upon IFN-β treatment; for qPCR on PIC-treated samples, ACTB was unsuitable for normalization as RNaseL activation degrades mRNA[28]. For these samples, we normalized gene expression of the lncRNA MALAT1, which is nuclear and its expression level insensitive to RNaseL activation. For all qPCR experiments, control reactions (no RT) were performed in the absence of cDNA for each primer pair, and confirmed to be negative.

Protein harvesting and Western-Blot

We first experimentally determined the linearity of all antibodies used in this study for the samples analyzed to allow for an adequate quantification in the linear range. For puromycin-incorporation assay, cells were treated with 10 µg/mL of puromycin for 10 min prior to harvesting, as previously described[36]. Cells were washed with PBS first and then lysed in RIPA buffer (150 mM NaCl, 1% NP-40, 0.5% Sodium Deoxycholate, 0.1% SDS, 50 mM Tris (pH 8.0), cOmplete Mini EDTA-free Protease Inhibitor Cocktail (Millipore Sigma) to 1x), 5 min on ice. For phosphorylated proteins, Halt Protease and Phosphatase Inhibitor Cocktail (ThermoFisher Scientific) was added to the RIPA buffer. DNA was fragmented using sonication at 30% amplitude for 1 min (10 seconds on, 10 seconds off using a qSonica sonicator. Lysates were then cleaned of debris by centrifugation at 13 000 RPM, 4°C, 10 min. Total protein content was measured using a standard Bradford assay. Samples were diluted in Laemmli buffer, heated at 95°C for 5 min and loaded on 10% or 6% SDS-polyacrylamide gels

alongside Precision Plus All Blue prestained protein ladder (Bio-Rad). Gels were transferred onto nitrocellulose membranes, blocked in 5% milk or BSA for 1 h and incubated with primary antibody diluted 1:1000 in blocking buffer overnight at 4°C. The commercial primary antibodies used in this study are the following: Actin (Sigma, A5441), eIF2α (Cell Signaling Technology, 9722S), p-eIF2α (Cell Signaling Technology, 9721S), PKR (Cell Signaling Technology, 12297), p-PKR (Abcam, ab32036), puromycin (Millipore Sigma, MABE343), RNaseL (Novus Biologicals, NBP2-80929), UPF1 (Cell Signaling Technology, 9435), p-UPF1 (Millipore Sigma, 07-1016), Vinculin (Santa Cruz Biotechnology, sc-73614). Blots were washed 3 x 5 min and incubated with Donkey Anti-Mouse or Anti-Rabbit IgG Polyclonal Antibody (IRDye® 800CW) for 1 h at room temperature. Membranes were washed again 3 times 5 min, and imaged on an Odyssey M Imaging System (LI-COR Biosciences). Images were analyzed with Empiria studio version 3.2 (LI-COR).

Immunofluorescence

A549 cells were seeded in 24-well plates on #1 glass coverslips (ThermoFisher Scientific) and treated as described in other sections. Cells were washed with PBS and fixed for 20 min using 4% paraformaldehyde in PBS (ThermoFisher Scientific). Cells were permeabilized in 0.15% triton X-100 (in PBS) for 5 min and then washed twice with PBS. Blocking was done in 10% goat serum (Gibco, diluted in PBS) for 20 min. Primary antibody against IRF3 (Cell Signaling, 11904) was diluted 1:250 in blocking buffer and incubated overnight at 4°C. Cells were washed in blocking buffer, three times, for 5 min. Goat anti-rabbit secondary antibody coupled to Alexa Fluor Plus 488 (ThermoFisher Scientific, A32731) was also diluted in blocking buffer (1:1000) and incubated 1 h in the dark. Cells were washed three time in PBS, and nuclei staining was performed using 1 µg/ml Hoechst 33342 in PBS for 15 min at room temperature. Coverslips were mounted on slides with SlowFade Diamond Antifade mounting medium (Invitrogen).

Microscopy imaging

Immunofluorescence experiments were imaged using a Zeiss LSM 980 confocal unit (50 µm pinhole size) attached to a Zeiss Axio Observer 7 inverted microscope. Images were acquired using a Plan Apochromat 63x/1.40 oil DIC M27 immersion objective, with a final pixel size of 0.071 µm/pixel. Green and Hoechst fluorescence were collected by illuminating the sample with a solid-state visible light laser at 488 nm and 405 nm, respectively. A 32-channel GaAsP-PMT detector was used to detect the emitted signal for Alexa Fluor 488, and a multialkali-PMT detector was used for Hoechst. The images were captured bidirectionally, with a pixel dwell time of 0.55 µs, a 1 AU pinhole and a repeat per line averaging using the mean intensity. ZEN Blue (v. 3.5, Zeiss) was used to acquire the data which was saved in the czi file format.

Data analysis and statistical analyses

All statistical analyses were performed using GraphPad Prism (version 10.4.2). Except were stated otherwise, the statistical results presented are ordinary one-way ANOVA using Dunnett's multiple comparisons test against the control sample;

ns, $P > 0.05$; *$P \leq 0.05$; **$P \leq 0.01$; ***$P \leq 0.001$; ****$P \leq 0.0001$. All results presented in this article are mean ± standard deviation.

RESULTS

EIF4A2 exon 10B is representative of NMD-targeted isoforms accumulating during viral infections

A well-documented role of NMD in cells is to reduce the abundance of alternative spliced products that generate premature stop codons, in a process known as AS-NMD[7–9]. Given that viral infection has been reported to have a broad impact on alternative splicing[12,14] and to inhibit NMD[17,18,20], we first asked if some of previously observed viral-induced alternative splicing changes might be attributable to accumulation of NMD-targeted isoforms. Indeed, we find that roughly 30% of alternative splicing changes triggered by Influenza A Virus (IAV)[13], as well as triggered by Vesicular Stomatitis Virus (VSV), are also observed in response to NMD inhibition (**Figure 1A**). This significant proportion of alternative splicing changes as NMD-sensitive suggests viral infection has a profound and broad effect on the NMD process leading to an accumulation of spliced transcripts that would normally be removed by NMD.

To further investigate the phenomena of AS-NMD in viral infection, we selected two previously characterized examples of AS-NMD, inclusion of alternative exon 10B in EIF4A2, and a differential 5'-SS usage in CDKN2AIP (**Figure 1B and Supplementary Figure S1A**). Both of these AS-NMD isoforms have previously been described to be induced upon infection with reovirus and IAV[10,11,13] and EIF4A2 exon 10B accumulation was also recently observed during coronavirus infection[37]. To expand these previous results we quantified splicing in A549 cells infected with a broad range of RNA viruses encompassing prototypical negative-strand RNA viruses (−ssRNA viruses; Vesicular Stomatitis Virus; VSV, a vesiculovirus, Rift Valley Fever Virus; RVFV, a phlebovirus; and Influenza A Virus, IAV, an orthomyxovirus), and positive-strand RNA viruses (+ssRNA viruses; West Nile Virus; WNV and Zika virus; ZIKV, two flaviviruses, and Chikungunya virus; CHIKV and Mayaro virus; MAYV, two togaviruses). RNA was harvested 24 h post-infection and subjected to RT-PCR to monitor the inclusion of EIF4A2 exon 10B and the alternate 5'-SS use in CDKN2AIP. All of the viruses tested, with the partial exception of CHIKV, showed a significant

increase in exon 10B inclusion following infection and differential 5'-SS usage in CDKN2AIP (**Figure 1C, Supplementary Figure S1B**). The percent spliced-in (PSI) metric was used to quantitate the level of inclusion in these alternative splicing events; it represents the percentage of the long form (10B included) over total abundance (both 10B included and 10B excluded). Viral replication was required to induce these AS-NMD isoforms, as UV-inactivated viruses were unable to trigger changes in isoform expression of EIF4A2 or CDKN2AIP (**Figure 1D, Supplementary Figure S1C**). Increased 10B inclusion could also be observed in VSV-infected HEK 293T or murine L929 fibroblasts, arguing against a cell-type specific effect observed only in A549 (**Supplementary Figure S2**).

To additionally confirm that 10B inclusion triggers NMD in our system, we first monitored the responsiveness of 10B to translation inhibition, since active translation is required for NMD[1]. Consistently, treatment of A549 cells with the translation inhibitors cycloheximide or homoharringtonine triggered 10B accumulation (**Figure 1E**). As further demonstration that inhibition of NMD leads to increased abundance of EIF4A2 exon 10B inclusion, we treated A549 cells with an inhibitor of SMG1 (SMG1i), the kinase responsible for phosphorylation of UPF1 as the first step for NMD[38]. Upon treatment with increasing SMG1i concentrations, we observe a dose-dependent increase in 10B inclusion, confirming that 10B-containing transcripts are normally reduced by NMD in A549 cells (**Figure 1F**). Similar results were also obtained with the 5'-SS in CDKN2AIP (**Supplementary Figure S1D**). In conclusion, inclusion of EIF4A2 exon 10B or altered use of the regulated 5'-SS in CDKN2AIP target the resulting transcripts for NMD degradation and are representative NMD isoforms increasing following infection with numerous RNA viruses. As inclusion of EIF4A2 exon 10B is the most straightforward to quantify by RT-PCR, we use this isoform expression as a marker for NMD in our subsequent experiments.

DsRNA sensing increases EIF4A2 exon 10B inclusion by inhibiting NMD

The observation that changes in splicing associated with AS-NMD are triggered during infection by numerous different viruses, and that this

phenomenon is dependent on viral replication, suggests that all these viruses produce something that blocks NMD. Numerous viruses produce pathogen-associated molecular patterns (PAMP) such as dsRNA and 5' triphosphate RNA during replication that are sensed by the host cell[39]. To test if a PAMP might be at least one mechanism responsible for the inhibition of NMD, we transfected seven different commercially available PAMP in A549 and monitored their effect on NMD by assaying EIF4A2 exon 10B inclusion. Of all the PAMP tested, only poly(I:C) (PIC), a mimic of dsRNA, could robustly trigger increased 10B inclusion in A549, as well as in HEK 293T or L929 **(Figure 2A, Supplementary Figure S3**). A block in NMD by PIC treatment is consistent with reports that dsRNA sensing inhibits translation[29], which we confirmed in our system by puromycin-incorporation (**Figure 2B**). To further confirm that the effect of PIC on EIF4A2 exon 10B inclusion is attributable to inhibition of NMD, we monitored the level of phosphorylated UPF1 (pUPF1). As the first step of NMD is the phosphorylation of UPF1 by the SMG1 kinase, pUPF1 is a widely used readout for the level of steady-state decay by NMD[2]. Upon PIC transfection, we observed a 50% decrease in pUFP1, most readily observed upon accumulation of pUFP1 using the phosphatase inhibitors okadaic acid and calyculin[40] (**Figure 2C**). Finally, we analyzed publicly available RNA-Seq data from PIC-treated A549 cells and again find a high level of AS-NMD isoforms induced in response to PIC (**Figure 2D**). Together, these results show that upon sensing of dsRNA, decreased efficiency of translation and NMD correlates with an increase in abundance of NMD-targeted isoforms.

NMD inhibition during dsRNA sensing is mediated primarily by RNaseL, and, to a lesser extent, PKR

Having established in our system that dsRNA sensing leads to a blockade in NMD, we next sought to decipher the precise sensors responsible for this NMD inhibition. Since we hypothesize that this block in NMD is downstream of the translational inhibition, we turned our attention to two of the main factors controlling translation during dsRNA sensing, i.e. RNaseL and PKR. Upon

binding to dsRNA, 2'-5'-oligoadenylate synthetases (OAS1, OAS2, and OAS3) catalyze the production of 2'-5'-oligoadenylates that trigger the dimerization of RNaseL, a nonspecific RNase that cleaves rRNA, mRNA, and viral RNA. This widespread RNA cleavage by RNaseL hampers translation[28]. By contrast, PKR is directly activated by dsRNA and phosphorylates the translation initiation factor eIF2α, which potently inhibits translation[29].

We tested OAS1, OAS2, OAS3, RNaseL, and PKR A549 knockout (KO) cells for their capacity to increase EIF4A2 exon 10B inclusion upon PIC transfection (**Figure 3A**). In A549 cells, RNaseL activation has been demonstrated to be solely dependent on OAS3[30], which we also confirmed (**Supplementary Figure S4**). Accordingly, genetic ablation of RNaseL and OAS3 both lead to a roughly 50% reduction in the increase in exon 10B inclusion, suggesting that RNaseL activation at least partially mediates NMD inhibition, while knock out of OAS1 and OAS2 had no effect. Notably, PKR knockout also did not reduce the ability of PIC to trigger increased exon 10B inclusion. However, given the fact that RNaseL depletion only has a partial impact on exon 10B inclusion, we wondered if PKR could be compensating in the absence of RNaseL. Indeed, depletion of PKR using siRNA in OAS3 KO (**Figure 3B**, left) or RNaseL KO (**Figure 3B**, right) cells completely blocks any PIC-induced inclusion of exon 10B; PKR depletion using siRNA was confirmed by WB (**Supplementary Figure S5A).** We also assessed the impact of the depletion using siRNA of RNaseL in the A549 PKR KO cells; although the siRNA-mediated depletion of RNaseL does not completely abrogate RNaseL activity, in the absence of PKR a significant reduction of the impact on 10B could be observed (**Supplementary Figure S5A, B**). Together, these data suggest that RNaseL is the dominant driver of PIC-induced inhibition of AS-NMD, with PKR activity compensating for this effect in the absence of RNaseL activation.

Although EIF4A2 exon 10B inclusion is a reliable marker for NMD, we further confirmed that RNaseL and PKR indeed are altering NMD by assessing translation. RNaseL is responsible for the bulk of the translational blockade upon PIC transfection, mirroring its effect on EIF4A2 exon 10B inclusion (**Figure 3C**).

Additionally, we find that activation of RNaseL, as well as PKR and eIF2α phosphorylation correlates with the degree of impact on exon 10B inclusion in response to PAMP (**Figure 3D**). Specifically, we find that only PIC triggers strong RNaseL/PKR activation, with modest impact on RNaseL by Poly(A:U), 5'-PPP-hpRNA, as well as Poly(dA:dT) (**Figure 3D**).

Finally, to directly demonstrate if dsRNA sensing during infection mediates the effect on 10B inclusion, we turned to vaccinia virus, a dsRNA virus that replicates solely in the cytoplasm. Removal of E3L, a viral dsRNA/dsDNA binding protein, leads to enhance dsRNA sensing during infection as well as increased RNaseL activation[30]. We monitored exon 10B inclusion upon infection with WT as well as ΔE3L vaccinia virus and shown that 10B inclusion is significantly increased in the ΔE3L mutant together with strong RNaseL activation (**Figure 3E**). Altogether, these results support a model in which translational inhibition, driven mainly by RNaseL, and to some extend by PKR in the absence of RNaseL activation, are responsible for the accumulation of NMD isoforms upon dsRNA sensing.

NMD promotes the IFN response

The observation that NMD is inhibited during dsRNA sensing led us to question if this inhibition could be playing a functional role in the events that are triggered following dsRNA recognition and signalling. We first tested the impact of NMD inhibition on the interferon response using SMG1i. To this end, A549 cells were pre-treated with SMG1i or DMSO, stimulated using IFN-β, and induction of interferon-stimulated genes (ISG) was measured. Upon NMD inhibition by SMG1i, we observed no notable change in the induction of IFIT1 or IFIT2 (**Supplemental Figure S6A**). We next turned to investigating the early events leading to the production of type I interferons by stimulating cells with PIC, and again observed no impact of SMG1i on the PIC-induced expression of IFN- β or the downstream IFIT1/2 (**Supplemental Figure S6B**).

One possible cause of the lack of impact of SMG1i on the interferon pathway is our observation that NMD is strongly inhibited following PIC transfection

(**Figure 2A-C**); we thus wondered if the NMD inhibition already induced during PIC infection could mask the effect of SMG1i. To test this hypothesis, we leveraged our finding that PIC-induced inhibition of NMD is driven mainly by RNaseL, and to a lesser extent, by PKR (**Figure 3A, B**). We thus transfected WT, PKR KO, RNaseL KO, or RNaseL KO with PKR depletion cells with PIC, and assessed induction of IFN-β, IFIT1, and IFIT2 by qPCR. Notably, we observed a significant increase in the IFN-β and ISG induction in RNaseL KO, and RNaseL/PKR double-depleted cells, but not in PKR KO cells (**Figure 4A, white bars**). This result supports a model in which NMD inhibition during dsRNA sensing decreases the IFN response, and abrogation of the NMD inhibition by removal of RNaseL and PKR relives this restriction. The conclusion that NMD inhibition limits the interferon response is further supported by the fact that treatment of the RNaseL KO or RNaseL/PKR double-depleted cells with SMG1i significantly reduced IFN-β and ISG induction to a degree correlated with the amount of NMD (**Figure 4A, grey bars**). Therefore, in all of these experiments the degree of NMD inhibition is strongly correlated with the extent of the interferon response, and NMD is required for optimal IFN response induction.

We next sought to understand how NMD is exerting control on the IFN response. Since we observed concurrent decreases in IFN-β induction with ISG induction, we hypothesize that the effect of NMD is upstream of IFN-β induction. We thus monitored the impact of NMD on translocation of IRF3 in the nucleus, which is a driving step in IFN-β mRNA production. To test this, we assessed the impact of SMG1i on IRF3 translocation in RNaseL/PKR double-depleted A549 cells stimulated with PIC (**Figure 4B**). Upon treatment with SMG1i, we observed a significant reduction in the percentage of cells with nuclear IRF3, suggesting NMD inhibition acts upstream of the translocation of IRF3 in the nucleus **(Figure 4B)**. We also monitored IRF3 translocation in WT A549 cells upon PIC transfection; concurrent with the absence of effect of SMG1i in these cells on the IFN-β mRNA induction (**Figure 4A**, **Supplemental Figure S6B**), we didn't observe a statistically significant decrease in nuclear IRF3 (**Supplemental Figure S7**). Altogether, these results demonstrate that during dsRNA sensing,

NMD contributes to IFN-β induction, and this effect is upstream of IRF3 translocation to the nucleus.

NMD promotes dsRNA sensing

Since we observed the effect of NMD inhibition to be acting upstream of the translocation of IRF3, we wondered if NMD could also be contributing more broadly to dsRNA sensing. In addition to the IFN response, dsRNA also activates RNaseL as shown in **Figure 3D**. However, our PKR and RNaseL double-depleted cells used to study the impact of NMD on the interferon response don't allow us to question the activation of RNaseL. We thus reasoned that usage of less PIC could probably alleviate some of the effect on NMD without completely abrogating RNaseL activation and would provide a window in which to test the impact of NMD on RNaseL activation. We first assessed NMD using EIF4A2 exon 10B inclusion across a broad range of PIC concentrations and indeed found that PIC concentrations of less than 250 ng/mL exhibit reduced EIF4A2 exon 10B inclusion (**Figure 5A**). Once again, the impact of PIC on exon 10B inclusion was correlated with the level of RNaseL activation (**Supplemental Figure S8**). We then monitored RNaseL activation following PIC transfection across a broad range of concentrations, in the presence or absence of the NMD inhibitor SMG1i. Importantly, at these PIC concentrations below 250 ng/mL that don't fully inhibit NMD, we do observe that inhibition of NMD with SMG1i reduces RNaseL activation (**Figure 5B**). These results underscore that in addition to controlling the IFN response, NMD also controls other dsRNA-mediated processes such as RNaseL activation, and suggest the effect of NMD on dsRNA-mediated processes lies at the sensing step.

DISCUSSION

The conflicting roles of NMD during viral infection, presenting both proviral and antiviral effects[17–20], suggest that NMD has a deeper impact beyond our current understanding. Here we demonstrate, using an AS-NMD isoform in EIF4A2 as a readout for NMD, that dsRNA sensing inhibits NMD primarily

through RNaseL activation, and to a lesser extent through redundant activity of PKR. Conversely, we also show that NMD itself is important for dsRNA-mediated processes, and its inhibition decreases dsRNA sensing and subsequent triggering of the IFN response, as well as activation of RNaseL.

Inhibition of NMD has been widely reported to be induced upon viral infection[17–20]. The production of dsRNA by viruses[41,42], as well as translation inhibition triggered during their replication cycle[43], likely contributes to this NMD blockade. From a viral fitness perspective, our result support the antiviral role of NMD during viral infection, as it promotes the interferon response which limits viral replication (**Figure 4A, Figure 6**). This model is in agreement with the widespread observation of NMD inhibition by viruses, likely globally benefiting viral fitness[17–20]. Since NMD inhibition is proviral, tolerating some levels of dsRNA and translation inhibition during infection might even proves beneficial for viruses as a way to limit the antiviral cellular responses. However, the discovery of this negative feedback loop involving NMD fails to provide a clear explanation for the proviral role of NMD during some viral infections, such as HCV and HIV[24,25]. One possibility would be that the sensitivity to the IFN response might be at play; viruses with a low sensitivity to the IFN response would be also lowly sensitive to this negative feedback loop involving NMD and might have evolved further mechanisms to subvert NMD and make it pro-viral. NMD's impact likely extend to other cellular processes during viral infection, both in host pathways as well as in the viral replication cycle, and further meticulous studies will be required to decipher each respective contribution to the global output observed. Notably, since the role of NMD during DNA viruses and −ssRNA viruses such as IAV and VSV has been less studied, a better characterization of the role and status of NMD during these infections will be helpful[19].

Interestingly, we don't observe any effect of SMG1i on IFN-β induction at the highest PIC concentration (**Supplemental Figure S6B**), and RNaseL activation (**Figure 5B**). These results suggests that NMD inhibition triggered by

high levels of dsRNA already exerts the maximal effect on inhibiting the IFN response and RNaseL activation. The need to use systems with no/low NMD inhibition to decipher this feedback loop, such as the RNaseL/PKR double-depleted cells and lower levels of PIC, indicate that the inhibitory effect of NMD on these pathways happens at low level of inhibition and quickly reach a maximal effect. Moreover, it also suggests this feedback happens under physiological circumstances to fine-tune and limit the inflammation process, likely contributing with other control mechanisms to the overall prevention of over activation. Limited evidence of the control of inflammation by NMD has been shown in human[44,45], but some evidence exist in plants[46,47]. Further studies should aim to decipher more broadly the role of NMD in inflammation and immunity.

We have shown that the effect of NMD is upstream of both IRF3 translocation to the nucleus (**Figure 4B**) as well as RNaseL activation (**Figure 5B**). These data suggest that NMD inhibition directly limits the sensing of dsRNA by the canonical sensors triggering the interferon response (RIG-1, MDA-5) as well as OAS3 responsible for RNaseL activation. However, we haven't established the molecular mechanism explaining this limitation in dsRNA sensing. One interesting hypothesis is that this effect is mediated by UPF1, the central helicase involved in NMD[48]. In our model of dsRNA sensing using PIC, UPF1 phosphorylation is inhibited (**Figure 2C**). Upon phosphorylation, UPF1 stays on the mRNA as the RNA is being degraded[2]. A decrease in pUPF1 would mean less UPF1 staying on the NMD-targeted RNA as they are being degraded, and a bigger pool of free UPF1. Moreover, RNaseL activation cleaves most of the cellular mRNA[28] resulting in a drastic depletion of mRNA, which would leave UPF1 without any target to bind to, once again contributing to more free UPF1. Interestingly, it has been observed that UPF1 binds to the viral RNA of SARS-CoV-2[49,50], as well as dsRNA in the context of uninfected cells[51–53] and during Sindbis virus infection[54]. Two different modes of action could explain our observations. First, upon RNaseL activation and decreases in phosphorylation, increased free UPF1 could bind and unwind dsRNA, leaving less dsRNA

molecules available to be sensed by the classical sensors responsible for triggering the IFN response and dsRNA-mediated processes. Second, UPF1 could also simply compete with these receptors for the binding to dsRNA without any unwinding activity and decreases sensing simply through competition. Further studies should aim to clarify the molecular mechanisms allowing NMD to control dsRNA sensing.

In conclusion, we have established that NMD is inhibited during dsRNA sensing, and this inhibition limits the induction of the interferon response (**Figure 6**). The main functional driver of this dsRNA-induced NMD inhibition is RNaseL, as removal of RNaseL increases the induction of the interferon response without a significant contribution of PKR (**Figure 4A**). This is intriguing as most viruses don't activate RNaseL[30]. However, it has already been shown that viruses such as WNV exert direct influence on the NMD machinery[16]. Moreover, we have also shown that in the absence of RNaseL, PKR activation drives at least some inhibition of NMD (**Figure 3A, 3B**). Therefore, we conclude that the precise mechanism by which NMD inhibition is achieved likely varies in a virus-specific manner, and further studies should aim to precisely decipher the status of NMD in viral-infected cells, the respective roles of RNaseL and PKR in these systems, and potential contributions from alternative splicing and other mechanisms to the accumulation of these NMD isoforms. However, our data demonstrates that regardless of the mechanism by which inhibition of NMD is achieved, at least one consequence is the attenuation of further dsRNA sensing. Therefore, we have uncovered a negative feedback loop in innate immune sensing involving NMD that contributes to fine-tuning the cellular response to dsRNA and, likely, viral infection.

ACKNOWLEDGEMENT

We thank Dr. Susan Weiss for providing the A549 KO cell lines. We would like to thank the CDB Microscopy Core (RRID SCR_022373) for providing access to confocal microscopes as well as technical help and training. We also thank Dr.

Sara Cherry and Mark Dittmar for providing RNA from infected cells. FUNDING – This work was supported by R35 GM118048 to KWL and a Banting scholarship from the Canadian Institutes of Health Research (CIHR), as well as postdoctoral scholarships from the Fonds de recherche du Québec – Santé (FRQ-S) and from the CIHR to S.B.

AUTHOR CONTRIBUTIONS

Conceptualization: SB, KWL; Data curation: SB, YR, MBF, JB; Formal analysis: SB, YR, MBF, JB; Funding acquisition: KWL; Investigation: SB, KWL; Methodology: SB, YR, KWL; Project administration: KWL; Resources: BLJ, KWL; Software: MBF; Supervision: SB, BLJ, KWL; Validation: SB, YR; Visualization: SB, MBF; Writing – original draft: SB, KWL; Writing – review & editing: SB, YR, MBF, JB, BLJ, KWL.

REFERENCES

1. He, F. & Jacobson, A. Nonsense-Mediated mRNA Decay: Degradation of Defective Transcripts Is Only Part of the Story. *Annual Review of Genetics* **49**, 339–366 (2015).
2. Kurosaki, T. *et al.* A post-translational regulatory switch on UPF1 controls targeted mRNA degradation. *Genes Dev.* **28**, 1900–1916 (2014).
3. Yamashita, A., Ohnishi, T., Kashima, I., Taya, Y. & Ohno, S. Human SMG-1, a novel phosphatidylinositol 3-kinase-related protein kinase, associates with components of the mRNA surveillance complex and is involved in the regulation of nonsense-mediated mRNA decay. *Genes Dev.* **15**, 2215–2228 (2001).
4. Colombo, M., Karousis, E. D., Bourquin, J., Bruggmann, R. & Mühlemann, O. Transcriptome-wide identification of NMD-targeted human mRNAs reveals extensive redundancy between SMG6- and SMG7-mediated degradation pathways. *RNA* **23**, 189–201 (2017).
5. Muñoz, O., Lore, M. & Jagannathan, S. The long and short of EJC-independent nonsense-mediated RNA decay. *Biochemical Society Transactions* BST20221131 (2023) doi:10.1042/BST20221131.
6. Kurosaki, T., Popp, M. W. & Maquat, L. E. Quality and quantity control of gene expression by nonsense-mediated mRNA decay. *Nat Rev Mol Cell Biol* **20**, 406–420 (2019).
7. Saltzman, A. L. *et al.* Regulation of Multiple Core Spliceosomal Proteins by Alternative Splicing-Coupled Nonsense-Mediated mRNA Decay. *Molecular and Cellular Biology* **28**, 4320–4330 (2008).

8. Frankiw, L., Mann, M., Li, G., Joglekar, A. & Baltimore, D. Alternative splicing coupled with transcript degradation modulates OAS1g antiviral activity. *RNA* **26**, 126–136 (2020).
9. Ni, J. Z. *et al.* Ultraconserved elements are associated with homeostatic control of splicing regulators by alternative splicing and nonsense-mediated decay. *Genes Dev.* **21**, 708–718 (2007).
10. Boudreault, S. *et al.* Global Profiling of the Cellular Alternative RNA Splicing Landscape during Virus-Host Interactions. *PLoS One* **11**, e0161914 (2016).
11. Boudreault, S. *et al.* Reovirus μ2 protein modulates host cell alternative splicing by reducing protein levels of U5 snRNP core components. *Nucleic Acids Res.* **50**, 5263–5281 (2022).
12. Boudreault, S., Roy, P., Lemay, G. & Bisaillon, M. Viral modulation of cellular RNA alternative splicing: A new key player in virus–host interactions? *Wiley Interdiscip. Rev. RNA* **10**, e1543 (2019).
13. Thompson, M. G. *et al.* Viral-induced alternative splicing of host genes promotes influenza replication. *eLife* **9**, e55500 (2020).
14. Mann, J. T., Riley, B. A. & Baker, S. F. All differential on the splicing front: Host alternative splicing alters the landscape of virus-host conflict. *Seminars in Cell & Developmental Biology* **146**, 40–56 (2023).
15. Balistreri, G. *et al.* The Host Nonsense-Mediated mRNA Decay Pathway Restricts Mammalian RNA Virus Replication. *Cell Host & Microbe* **16**, 403–411 (2014).
16. Li, M. *et al.* Identification of antiviral roles for the exon–junction complex and nonsense-mediated decay in flaviviral infection. *Nat Microbiol* **4**, 985–995 (2019).
17. Ahmed, M. R. & Du, Z. Molecular Interaction of Nonsense-Mediated mRNA Decay with Viruses. *Viruses* **15**, 816 (2023).
18. Popp, M. W.-L., Cho, H. & Maquat, L. E. Viral subversion of nonsense-mediated mRNA decay. *RNA* **26**, 1509–1518 (2020).
19. van der Klugt, T. & van Gent, M. The dynamic interactions between virus infections and nonsense-mediated decay. *Human Molecular Genetics* ddae151 (2025) doi:10.1093/hmg/ddae151.
20. Leon, K. & Ott, M. An ‘Arms Race’ between the Nonsense-mediated mRNA Decay Pathway and Viral Infections. *Seminars in Cell & Developmental Biology* **111**, 101–107 (2021).
21. Contu, L., Balistreri, G., Domanski, M., Uldry, A.-C. & Mühlemann, O. Characterisation of the Semliki Forest Virus-host cell interactome reveals the viral capsid protein as an inhibitor of nonsense-mediated mRNA decay. *PLOS Pathogens* **17**, e1009603 (2021).
22. Mallick, M. *et al.* Modulation of UPF1 catalytic activity upon interaction of SARS-CoV-2 Nucleocapsid protein with factors involved in nonsense mediated-mRNA decay. *Nucleic Acids Research* **52**, 13325–13339 (2024).
23. Nuccetelli, V. *et al.* The SARS-CoV-2 nucleocapsid protein interferes with the full enzymatic activation of UPF1 and its interaction with UPF2. *Nucleic Acids Research* **53**, gkaf010 (2025).

24. Ramage, H. R. *et al.* A Combined Proteomics/Genomics Approach Links Hepatitis C Virus Infection with Nonsense-Mediated mRNA Decay. *Molecular Cell* **57**, 329–340 (2015).
25. Serquiña, A. K. P. *et al.* UPF1 Is Crucial for the Infectivity of Human Immunodeficiency Virus Type 1 Progeny Virions. *Journal of Virology* **87**, 8853–8861 (2013).
26. Tran, G. V. Q. *et al.* Nonsense-mediated mRNA decay does not restrict influenza A virus propagation. *Cellular Microbiology* **23**, e13323 (2021).
27. Fensterl, V., Chattopadhyay, S. & Sen, G. C. No Love Lost Between Viruses and Interferons. *Annu. Rev. Virol.* **2**, 549–572 (2015).
28. Karasik, A. & Guydosh, N. R. The Unusual Role of Ribonuclease L in Innate Immunity. *WIREs RNA* **15**, e1878 (2024).
29. Gal-Ben-Ari, S., Barrera, I., Ehrlich, M. & Rosenblum, K. PKR: A Kinase to Remember. *Front. Mol. Neurosci.* **11**, (2019).
30. Li, Y. *et al.* Activation of RNase L is dependent on OAS3 expression during infection with diverse human viruses. *Proceedings of the National Academy of Sciences* **113**, 2241–2246 (2016).
31. Li, Y. *et al.* Ribonuclease L mediates the cell-lethal phenotype of double-stranded RNA editing enzyme ADAR1 deficiency in a human cell line. *eLife* **6**, e25687 (2017).
32. Beattie, E. *et al.* Reversal of the interferon-sensitive phenotype of a vaccinia virus lacking E3L by expression of the reovirus S4 gene. *Journal of Virology* **69**, 499–505 (1995).
33. Tartaglia, J. *et al.* NYVAC: A highly attenuated strain of vaccinia virus. *Virology* **188**, 217–232 (1992).
34. Ip, J. Y. *et al.* Global analysis of alternative splicing during T-cell activation. *RNA* **13**, 563–572 (2007).
35. Rothrock, C., Cannon, B., Hahm, B. & Lynch, K. W. A Conserved Signal-Responsive Sequence Mediates Activation-Induced Alternative Splicing of CD45. *Molecular Cell* **12**, 1317–1324 (2003).
36. Schmidt, E. K., Clavarino, G., Ceppi, M. & Pierre, P. SUnSET, a nonradioactive method to monitor protein synthesis. *Nat Methods* **6**, 275–277 (2009).
37. Bresson, S., Sani, E., Armatowska, A., Dixon, C. & Tollervey, D. The transcriptional and translational landscape of HCoV-OC43 infection. *PLOS Pathogens* **21**, e1012831 (2025).
38. Gopalsamy, A. *et al.* Identification of pyrimidine derivatives as hSMG-1 inhibitors. *Bioorganic & Medicinal Chemistry Letters* **22**, 6636–6641 (2012).
39. Jensen, S. & Thomsen, A. R. Sensing of RNA Viruses: a Review of Innate Immune Receptors Involved in Recognizing RNA Virus Invasion. *J Virol* **86**, 2900–2910 (2012).
40. Ishihara, H. *et al.* Calyculin A and okadaic acid: Inhibitors of protein phosphatase activity. *Biochemical and Biophysical Research Communications* **159**, 871–877 (1989).
41. Weber, F., Wagner, V., Rasmussen, S. B., Hartmann, R. & Paludan, S. R. Double-Stranded RNA Is Produced by Positive-Strand RNA Viruses and DNA

Viruses but Not in Detectable Amounts by Negative-Strand RNA Viruses. *Journal of Virology* **80**, 5059–5064 (2006).
42. Son, K.-N., Liang, Z. & Lipton, H. L. Double-Stranded RNA Is Detected by Immunofluorescence Analysis in RNA and DNA Virus Infections, Including Those by Negative-Stranded RNA Viruses. *Journal of Virology* **89**, 9383–9392 (2015).
43. Rozman, B., Fisher, T. & Stern-Ginossar, N. Translation—A tug of war during viral infection. *Molecular Cell* **83**, 481–495 (2023).
44. Oliveira, V. *et al.* A Protective Role for the Human SMG-1 Kinase against Tumor Necrosis Factor-α-induced Apoptosis *. *Journal of Biological Chemistry* **283**, 13174–13184 (2008).
45. Johnson, J. L. *et al.* Inhibition of Upf2-Dependent Nonsense-Mediated Decay Leads to Behavioral and Neurophysiological Abnormalities by Activating the Immune Response. *Neuron* **104**, 665-679.e8 (2019).
46. Gloggnitzer, J. *et al.* Nonsense-Mediated mRNA Decay Modulates Immune Receptor Levels to Regulate Plant Antibacterial Defense. *Cell Host & Microbe* **16**, 376–390 (2014).
47. Nasim, Z., Karim, N., Blilou, I. & Ahn, J. H. NMD-mediated posttranscriptional regulation fine-tunes the NLR-WRKY regulatory module to modulate bacterial defense response. *Plant Sci* **356**, 112528 (2025).
48. Weng, Y., Czaplinski, K. & Peltz, S. W. Genetic and Biochemical Characterization of Mutations in the ATPase and Helicase Regions of the Upf1 Protein. *Molecular and Cellular Biology* (1996) doi:10.1128/MCB.16.10.5477.
49. Lee, S. *et al.* The SARS-CoV-2 RNA interactome. *Molecular Cell* **81**, 2838-2850.e6 (2021).
50. Schmidt, N. *et al.* The SARS-CoV-2 RNA–protein interactome in infected human cells. *Nat Microbiol* **6**, 339–353 (2021).
51. Lim, J. *et al.* Cellular dsRNA interactome captured by K1 antibody reveals the regulatory map of exogenous RNA sensing. *Commun Biol* **8**, 1–12 (2025).
52. Pennemann, F. L. *et al.* Cross-species analysis of viral nucleic acid interacting proteins identifies TAOKs as innate immune regulators. *Nat Commun* **12**, 7009 (2021).
53. Fischer, J. W., Busa, V. F., Shao, Y. & Leung, A. K. L. Structure-Mediated RNA Decay by UPF1 and G3BP1. *Molecular Cell* **78**, 70-84.e6 (2020).
54. Girardi, E. *et al.* Proteomics-based determination of double-stranded RNA interactome reveals known and new factors involved in Sindbis virus infection. *RNA* **29**, 361–375 (2023).

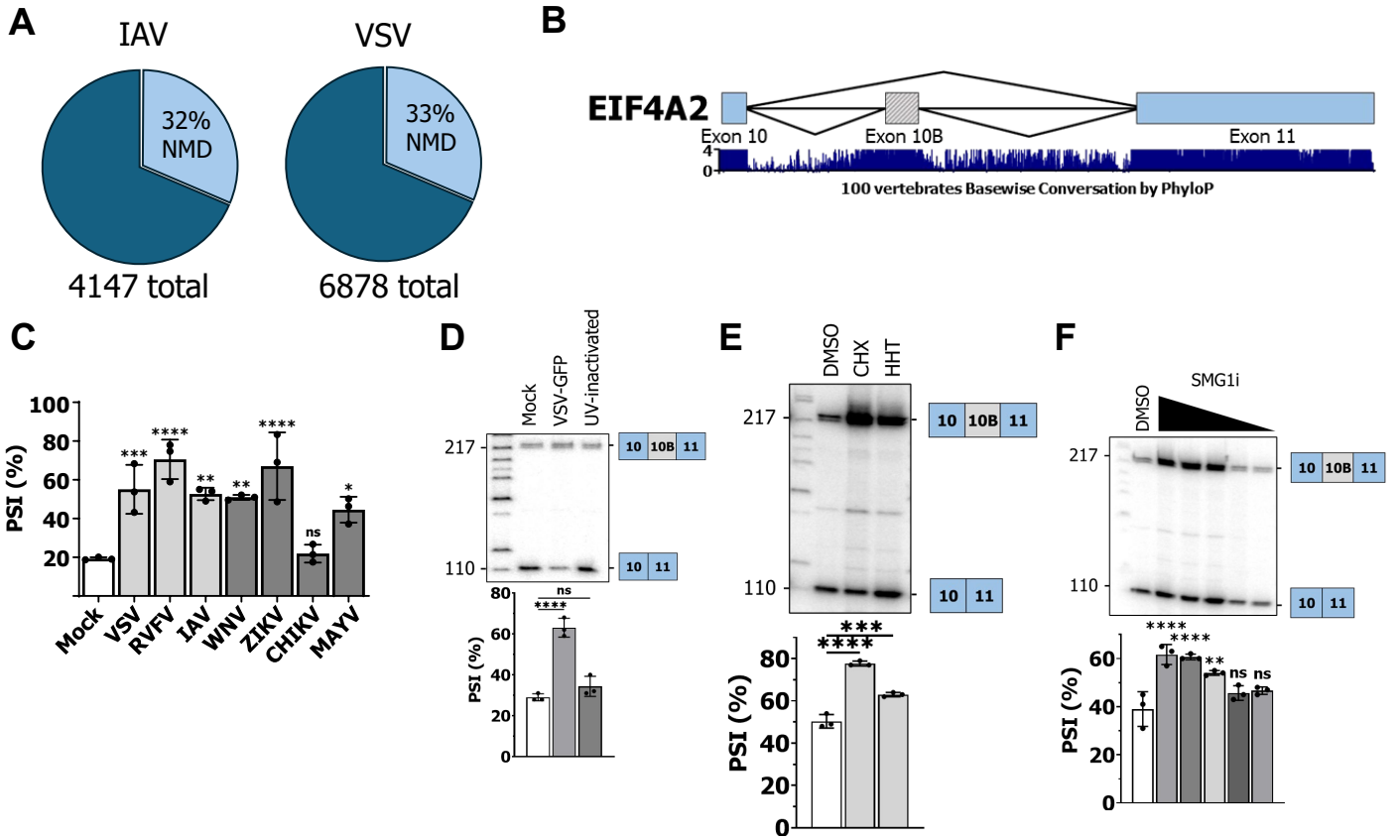

Figure 1. EIF4A2 exon 10B is representative of NMD-targeted isoforms accumulating during viral infections. (A) Widespread accumulation of NMD isoforms upon infection with Influenza A virus (IAV) and Vesicular Stomatitis Virus (VSV). A549 cells were infected for 12 h (IAV) or 24 h (VSV), RNA sequenced, splicing analyzed using MAJIQ and NMD isoforms determined from NMD datasets (see material and methods). (B) Schematic of the exon 10B splicing in EIF4A2. Conservation values across 100 vertebrates is shown underneath. (C) Impact of viral infection with prototypical -ssRNA viruses (Vesicular Stomatitis Virus (VSV), Rift Valley Fever Virus (RVFV), and Influenza A Virus (IAV)) and +ssRNA viruses (West Nile Virus (WNV), Zika virus (ZIKV), Chikungunya virus (CHIKV), and Mayaro virus (MAYV) on EIF4A2 exon 10B inclusion. A549 cells were infected at a MOI of 5, RNA harvested at 24 h PI and subjected to radiolabelled RT-PCR for EIF4A2 exon 10B inclusion. (D) Impact of VSV and UV-inactivated VSV on EIF4A2 exon 10B splicing. (E) EIF4A2 exon 10B accumulates following translation inhibition. A549 cells were treated with DMSO, cycloheximide (CHX), or homoharringtonine (HHT) for 5h. RNA was harvested and subjected to radiolabelled RT-PCR for EIF4A2 exon 10B inclusion. (F) EIF4A2 exon 10B accumulates following NMD inhibition. A549 cells were treated with DMSO or SMG1i, a SMG1i inhibitor, at 3 μM, 1 μM, 300 nM, 100 nM, or 30 nM, for 7h. RNA was harvested and subjected to radiolabelled RT-PCR for EIF4A2 exon 10B inclusion.

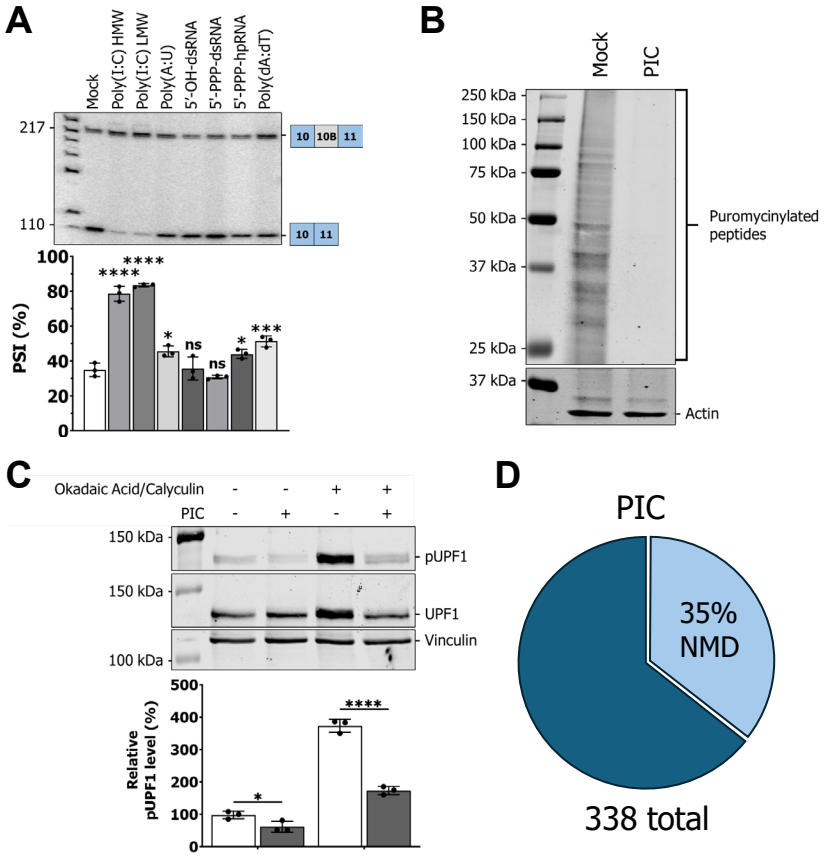

Figure 2. dsRNA sensing increases EIF4A2 exon 10B inclusion by inhibiting NMD. (A) Monitoring of EIF4A2 exon 10B inclusion following transfection of seven different PAMP in A549 cells for 6h. (B) Puromycin-incorporation assay of mock-transfected or PIC-transfected A549 cells. Cells were treated with 10 µg/mL of puromycin for 10 min, prior to western-blotting for puromycinylated peptides or actin loading control. (C) Western blot of pUPF1, UPF1, and vinculin (loading control) in A549 cells following poly(I:C) transfection. 50 nM calyculin and 500 nM okadaic acid were added 5 minutes prior to harvesting to prevent dephospholyration of UPF1 and increase the signal, where indicated. (D) Widespread accumulation of NMD isoforms upon PIC transfection. Publicly available datsets of PIC-transfected cells were analyzed using MAJIQ for alternative splicing and NMD isoforms determined from NMD datasets (see material and methods).

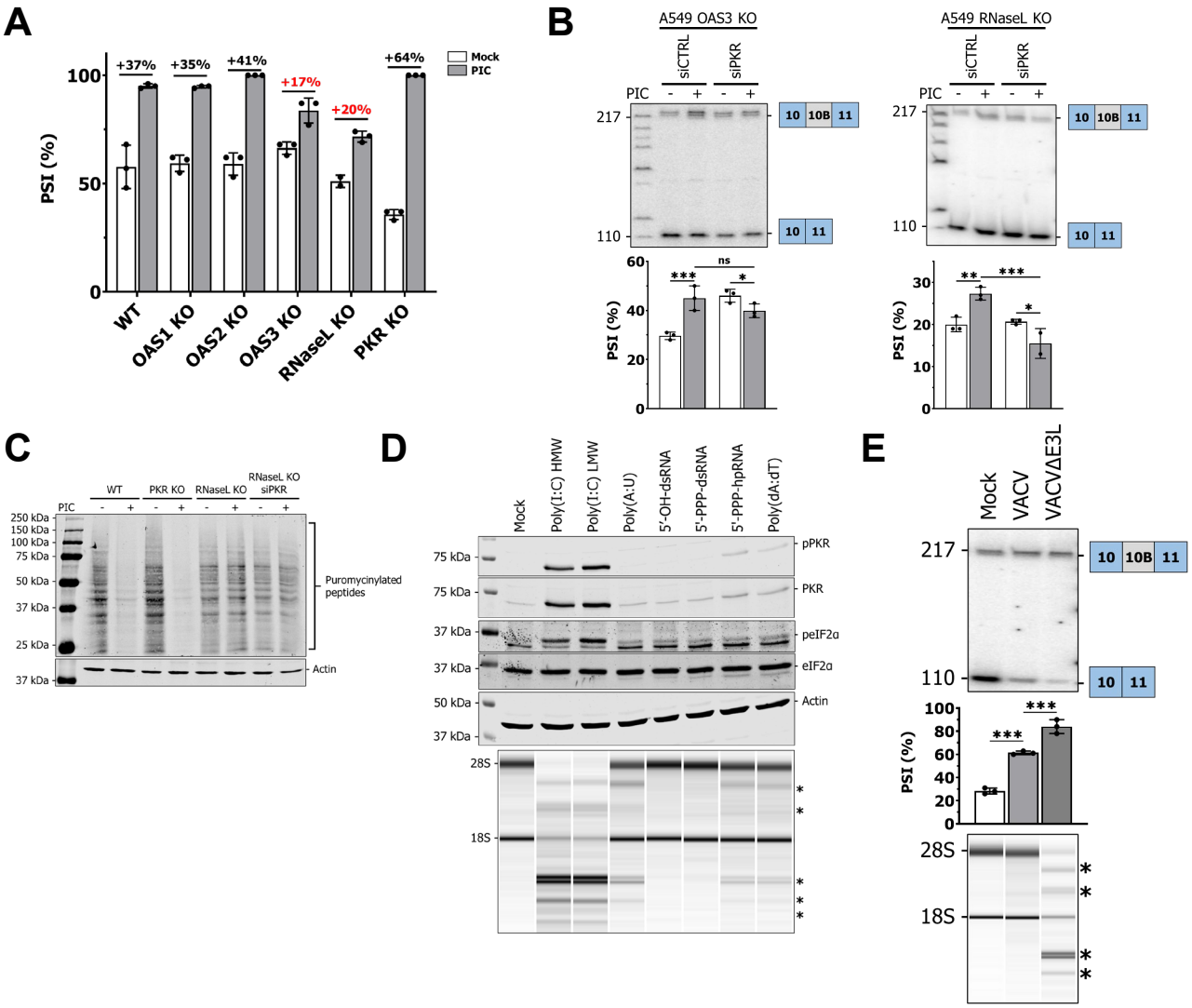

Figure 3. NMD inhibition during dsRNA sensing is mediated primarily by RNaseL, and, to a lesser extent, PKR. (A) Impact of PIC transfection on 10B inclusion in WT, OAS1, OAS2, OAS3, RNaseL, and PKR KO A549 cells. (B) siRNA-mediated depletion of PKR in OAS3 or RNaseL KO A549 cells. Cells were transfected with siRNA for 72h prior to be transfected with PIC for 6h and RNA harvested for EIF4A2 exon 10B radioactive RT-PCR. Two-way ANOVA with uncorrected Fisher's LSD multiple comparisons test. (C) Puromycin-incoroporation assay to measure translation in WT, PKR KO, RNaseL KO, and RNaseL KO + siPKR to monitor the translational output upon stimulation with PIC. (D) Monitoring PKR and RNaseL activation following PAMP transfection in A549. Top, western-blot for pPKR, total PKR, peIF2α, total eIF2α as well as actin (loading control). Bottom, total RNA was run on a Bioanalyzer to monitor RNaseL activation by monitoring rRNA cleavage. Asterisks denote the cleavage products of ribosomal RNA typical of RNaseL activation. (E) Monitoring WT vaccinia virus (VACV) or ΔE3L mutant (VACVΔE3L) impact on 10B inclusion. Top, radioactive RT-PCR for EIF4A2 exon 10B; bottom, total RNA on a Bioanalyzer to monitor RNaseL activation. Asterisks denote the cleavage products of ribosomal RNA typical of RNaseL activation. Ordinary one-way ANOVA using Tukey's multiple comparisons test.

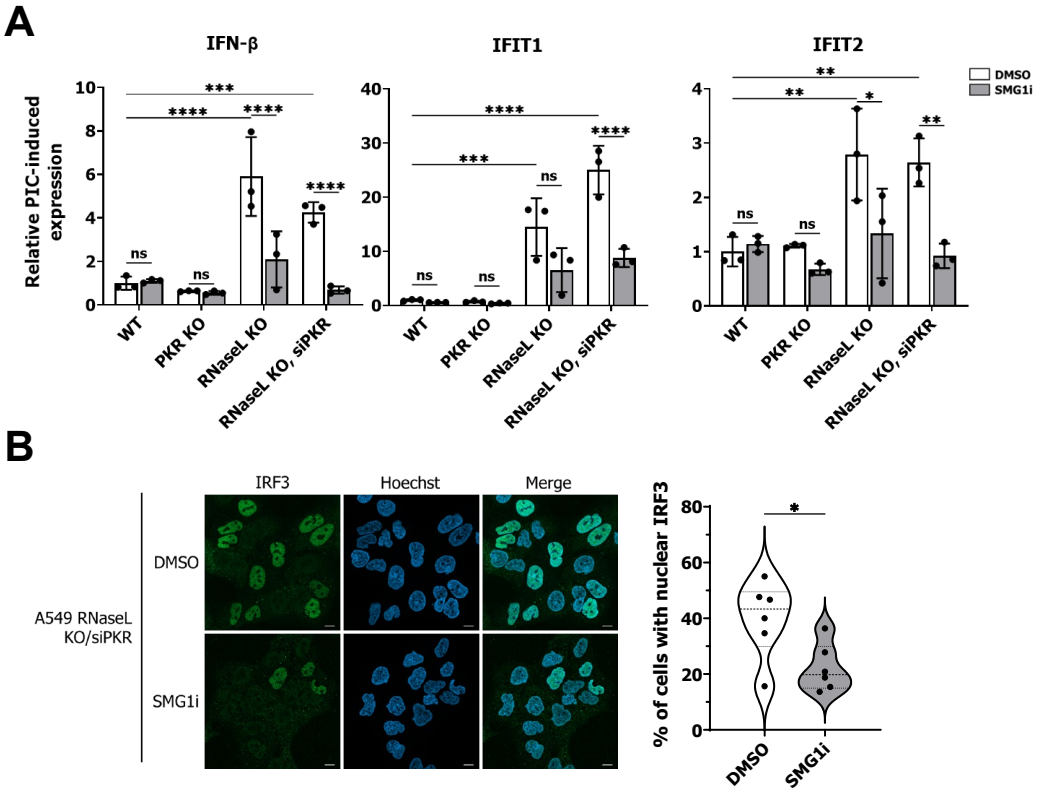

Figure 4. NMD promotes the IFN response. (A) A549 WT, PKR KO, RNaseL KO as well as RNaseL KO transfected with siRNA against PKR were pre-treated with DMSO or SMG1i (3 µM) for 1h and transfected with 1 µg of PIC and RNA harvested at 6h. Two-way ANOVA with uncorrected Fisher's LSD multiple comparisons test. (B) Left, immunofluorescence for IRF3 of DMSO or SMG1i-treated cells transfected with PIC. A549 RNaseL KO were transfected with siPKR for 72h, pre-treated with DMSO or SMG1i (3 µM) for 1h and transfected with 1 µg of PIC prior to IF. Scale bar, 10 µm. Right, quantification of the number of cells with IRF3 nuclear localization. 6 fields were counted for each condition each containing between 14 and 36 cells. Unpaired two-tailed Student's t-test.

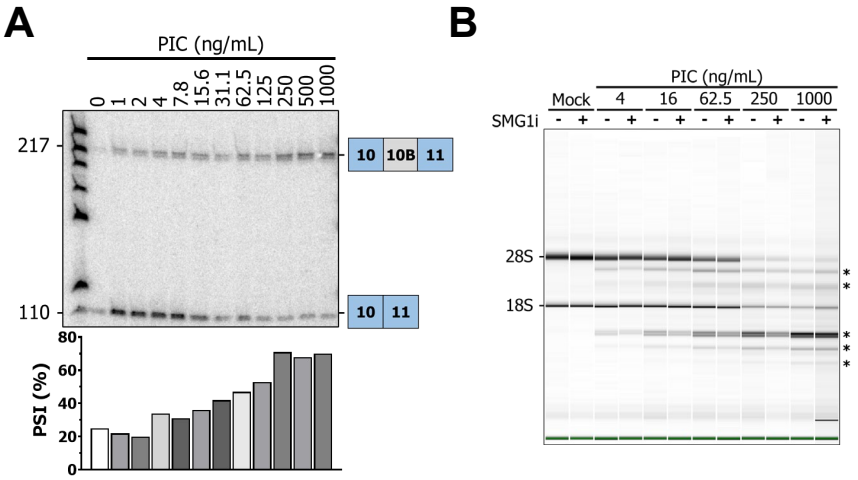

Figure 5. NMD promotes dsRNA sensing. (A) Monitoring of EIF4A2 exon 10B inclusion following transfection of increasing quantity of PIC. Between 0 ng/mL and 1000 ng/mL of PIC was transfected in A549 for 6h prior to RNA harvesting and RT-PCR for EIF4A2 exon 10B. (B) Impact of NMD inhibition on RNaseL activation. Cells were pre-treated for 1 h with DMSO or SMG1i (3 μM) prior to transfection of different quantity of PIC for 6 h; RNA was harvested and run on a Bioanalyzer. Asterisks denote the cleavage products of ribosomal RNA typical of RNaseL activation.

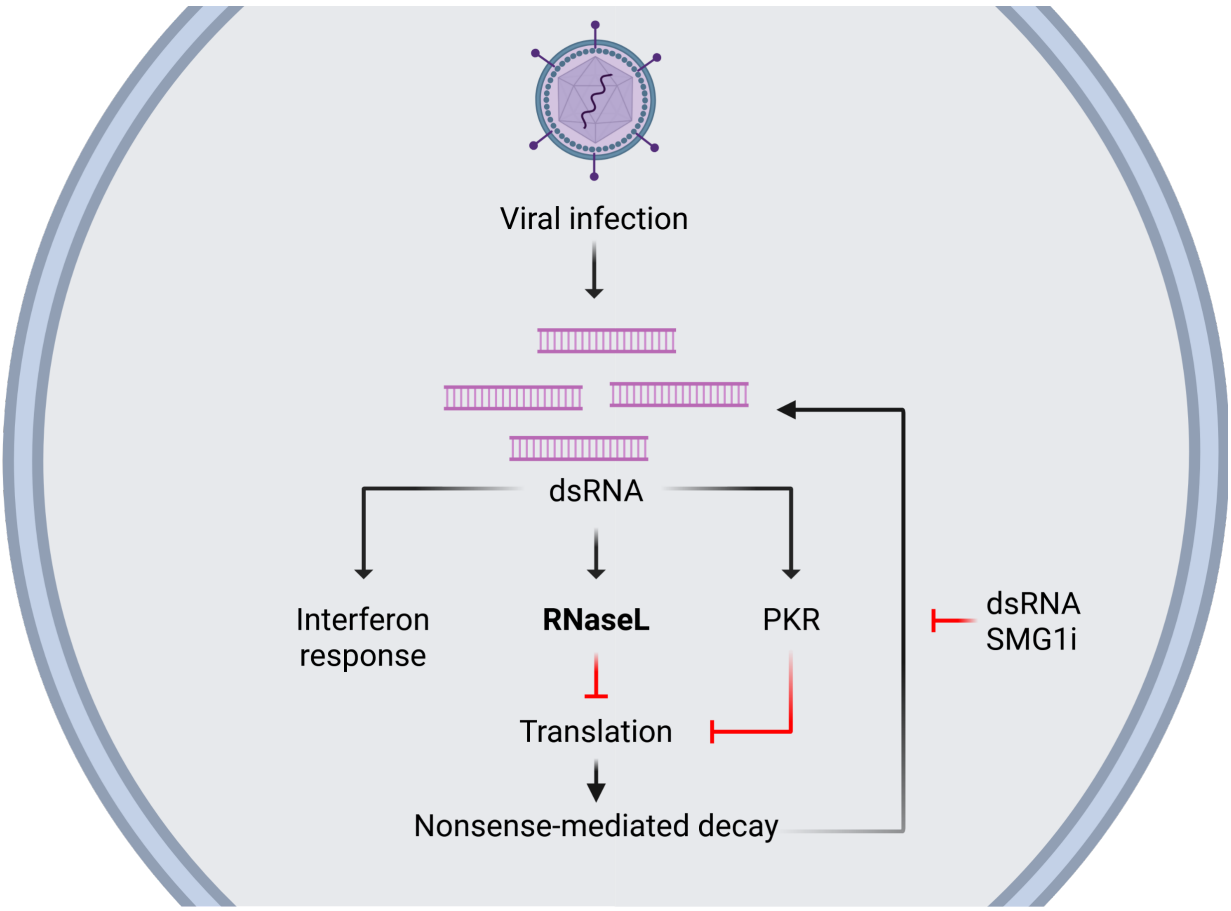

Figure 6. Model of the feedback loop involving NMD during dsRNA sensing. Upon viral infection, dsRNA is produced by most viral infections. This dsRNA, aside from triggering the innate immune sensing pathway and the interferon response, activates RNaseL and PKR, which drastically inhibits translation. In this state of stricking reduction of translation, NMD is also decreased, leading to the accumulation of NMD-decayed isoforms. These isoforms, or the inhibition of NMD itself, feeds back to limit the sensing of dsRNA, in a negative feedback look that will decrease the interferon response as well as RNaseL activation. Created in BioRender. Lynch, K. (2025) https://BioRender.com/3or17n1.